Coupled Systems Mechanics, *Vol. 13, No. 5 (2024) 459-470*
https://doi.org/10.12989/csm.2024.13.5.459

Analysis of 3D pendulum sliding along a rope

Ivica Kožar*

Faculty of Civil Engineering, Radmile Matejcic 3, Rijeka, Croatia

(Received August 9, 2024, Revised October 29, 2024, Accepted October 30, 2024)

Abstract. The paper deals with a dynamic engineering problem in which a mass attached to a pendulum slides along a cable. In this problem, the pendulum mass and the cable are coupled in a model described by a system of algebraic differential equations (DAE). In this paper, the formulation of the system of differential equations modelling the problem is presented together with the determination of the initial conditions. The developed model is general in the sense of a free choice of support location, elastic rope properties, pendulum length and the inclusion of braking forces. This model can be used in the design of real rope structures such as zip lines. Many calculated values that can be measured on a real structure can be exported from the model and used for parameter calibration. In one example, the model is related to a real rope structure to illustrate and validate the model. The most important aspect of the model is its ability to estimate the safety of a ropeway quickly and easily.

Keywords: differential algebraic equations; elastic 3D rope/cable; sliding 3D pendulum; sliding mass

1. Introduction

The article deals with a dynamic engineering problem in which a mass attached to a pendulum slides along an elastic rope. This type of problem describes many practical applications such as weight manipulation, construction site transportation, ropeways, etc.

Usually, the centre of gravity of the mass is outside the rope axis, which is modelled with a pendulum attached to the rope. A similar problem was analysed in Kožar and Torić Malić (2014) and this is the 3D extension of this work. Other authors have analysed similar problems, like Burov and Nikonov (2024) who have analyzed oscillations of a heavy pendulum with variable suspension length. Golub *et al.* (2023) deal with a multilink pendulum located in a flow. In Costa and Savi (2024) a pendulum model describes a multidirectional mechanical energy harvester. Ren *et al.* (2024) consider an inertial pendulum as the key part of a miniature wire suspended pendulum accelerometer.

The terms ‘cable’ and ‘rope’ are used interchangeably throughout the paper to emphasise that the cable in the model is massless.

The pendulum mass and the cable are coupled in a model described by a system of algebraic differential equations (DAE). The initial conditions for the given system of DAEs are formulated and solved separately. From the literature, finite elements are the preferred method for solving

*Corresponding author, Professor, E-mail: ivica.kozar@gradri.uniri.hr, ivica.kozar.gradri@gmail.com

http://www.techno-press.org/?journal=csm&subpage=8 ISSN: 2234-2184 (Print), 2234-2192 (Online)

Table 1 Description of the variables used in the model

a - position on the rope	u - longitudinal velocity of rope at 'a'
F - displacement of the rope at 'a'	v - vertical velocity of rope at 'a'
Y - lateral displacement of the rope at 'a'	w - lateral velocity of rope at 'a'
ϑ - pendulum angle along to the rope	p - velocity (speed of change) of ϑ
ψ - pendulum angle perpendicular to the rope	q - velocity (speed of change) of ψ
EA - cable elastic properties	L - cable length ($L=L_1+L_2$)
m - mass of the sliding body	l - projected cable length
T - tension force in the cable	h - height between cable supports

structural problems, but here the moving mass is a part of the structure, which requires the development of special finite elements (Zhou *et al.* 2004). However, searching the available sources, no finite element formulation was found that takes into account the mass suspended from a pendulum and realistically describes the engineering problem of a sliding body. No analytical formulation of the problem can be found in the literature. Note that the sliding along the wire should be distinguished from the sliding of the wire itself (Coulibaly *et al.* 2018). In the sliding mass problem, there is no equilibrium without the sliding mass, i.e., the wire and the mass are coupled into a system of algebraic differential equations (the wire imposes nonlinear constraints on the dynamic equations of mass motion).

A numerical procedure suitable for solution of the problem is not the subject of the paper. However, one could apply different numerical methods like Elhoucin *et al.* (2021) that use a novel time stepping algorithm for a nonlinear dynamic problem. This problem is described as a deterministic one but stochastic approach could be developed like in Ibrahimbegovic *et al.* (2022).

We have developed a novel analytical model for a mass attached to a pendulum sliding along a three-dimensional massless wire or cable. Since we want to solve a real engineering problem, it is important to take into account the elastic properties of the rope (elongation of the rope under tensile load). The developed model is general in the sense of the free choice of the support point, the elastic rope properties, the pendulum length and the inclusion of the braking forces (or the friction coefficient). A further generalisation would include several consecutive masses (Rukavina and Kožar 2017).

At the end of the paper you will find an example to check and illustrate the model. Some of the model results are presented graphically. They can be compared with field measurements and used for parameter calibration and rope/cable design improvement. Moreover, measured data could be used for an inverse analysis like in Suljevic *et al.* (2022) or Nguyen *et al.* (2022). One novel method of inverse analysis is presented in Kožar *et al.* (2022).

The novelty of the model is that it successfully describes a mass suspended from a 3D pendulum sliding along a 3D cable. This approach combines the two independent formulations: i) the sliding of a mass along an extensible 3D rope and ii) the motion of a 3D pendulum in the general translational coordinate system. Moreover, this analytical approach can be used to test different discrete formulations of the problem.

2. Sliding pendulum model

The rope imposes nonlinear constraints on the dynamic equations of a point mass sliding along

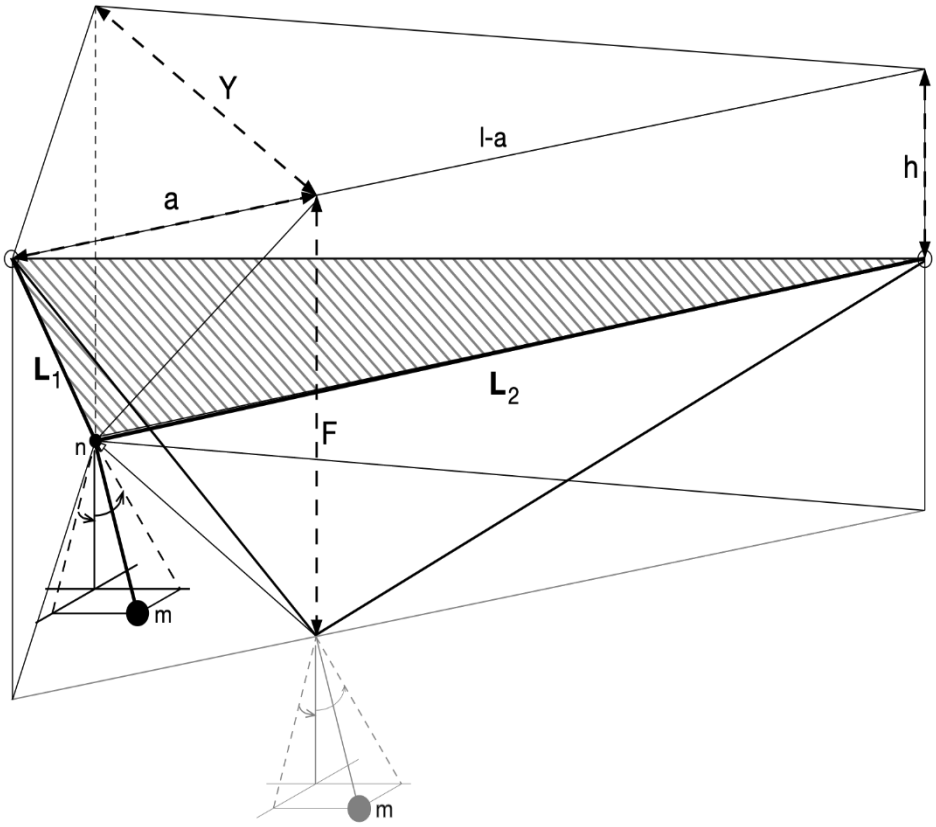

Fig. 1 Rope kinematics in 3D, '*n*' is the point where the pendulum is attached, for the rest see Table 1

the rope and creates a translational origin for the mass swinging on the pendulum. The 3D pendulum is modeled as a system of differential equations that have been modified to take into account the moving origin. The second system of differential equations stems from the moving origin along an elastic rope. The two systems of equations are combined into a system of 10 normalised, i.e., first-order algebraic differential equations.

See Table 1 for the meaning of the variables in Figs. 1 and 2.

2.1 The sliding mass model

The sliding mass model assumes a straight rope, i.e., the dead weight of the rope is neglected and the rope sag is rather small. This model is suitable for the analysis of light ropes and thin steel cables with very low sag. The description of the dynamic equilibrium of mass leads to three second-order differential equations relating the mass accelerations in three coordinate directions to the kinematic constraints of the rope. The kinematics of the model for the sliding of the mass along a rope/cable is shown in Fig. 1, and the model for a 3D pendulum suitable for connection with the sliding model is shown in Fig. 2. In Fig. 1 we see rope/cable together with its pendulum changing plane, from the vertical to the inclined. Lateral rope displacement 'Y 'turns a 2D model into a 3D one.

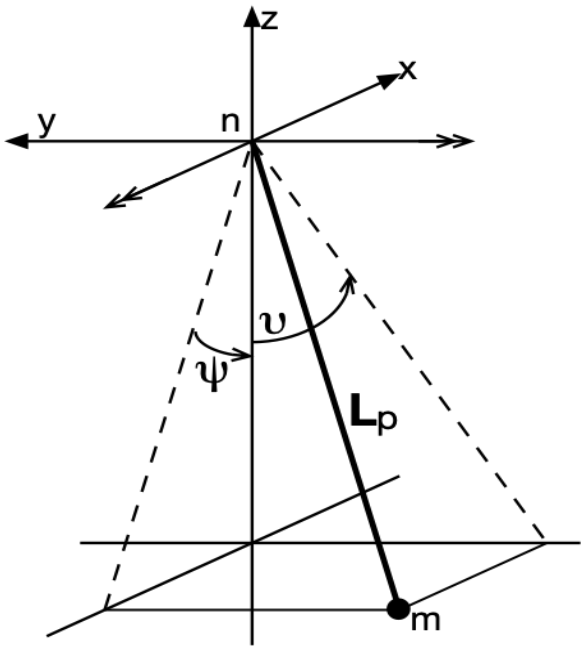

Fig. 2 Pendulum kinematics in 3D

In the case of a sliding mass, the force along the rope is constant. The differential equations describing the problem are (with the nomenclature from Fig. 1 and Table 1)

$$\begin{Bmatrix} \ddot{a} \\ \ddot{Y} \\ \ddot{F} \end{Bmatrix} = \begin{Bmatrix} DE_1 \\ DE_2 \\ DE_3 \end{Bmatrix} \tag{1}$$

where

$$DE_1 = \frac{EA}{m}\frac{L_1+L_2}{L-1}\left(\frac{l-a}{L_2}-\frac{a}{L_1}\right),\ DE_2 = \frac{G}{m}-\frac{EA}{m}\frac{L_1+L_2}{L-1}\left(\frac{F-h}{L_2}+\frac{F}{L_1}\right) \text{ and}$$

$$DE_3 = -\frac{EA}{m}\frac{L_1+L_2}{L-1}\left(\frac{Y}{L_2}+\frac{Y}{L_1}\right) \text{ and } \quad \ddot{a} = \frac{d^2a}{dt^2}\ ,\ddot{Y} = \frac{d^2Y}{dt^2}\ ,\ddot{F} = \frac{d^2F}{dt^2}\ .$$

The above equation is nonlinear because lengths 'L' are not constants but functions, i.e., $L_1 = L1(a,F,Y) = \sqrt{(a^2+F^2+Y^2)}$ and $L_2 = L2(a,F,Y) = \sqrt{(l-a)^2+(F-h)^2+Y^2}$.

2.2 The pendulum model

The pendulum model describes the 3D oscillation of a mass on an inextensible wire. The model is formulated in a local {x, y, z} coordinate system, where 'z' is not an independent coordinate because we have $z^2 = L_p^2 - x^2 - y^2$ due to the inextensible pendulum wire of length 'Lp'. The kinematics of the 3D pendulum suitable for connection to the sliding model is shown in Fig. 2. Note the point 'n' in Fig. 1 and Fig. 2 where the two models connect.

The relationship between the relative pendulum coordinates and the pendulum angles is as follows

$$\begin{Bmatrix} x \\ y \\ z \end{Bmatrix} = \left(E_\psi F_\vartheta\right)^{-1} \begin{Bmatrix} 0 \\ 0 \\ L_p \end{Bmatrix} \tag{2}$$

where $E_\psi = \begin{bmatrix} cos(\psi(t)) & 0 & -sin(\psi(t)) \\ 0 & 1 & 0 \\ sin(\psi(t)) & 0 & cos(\psi(t)) \end{bmatrix}$ and $F_\vartheta = \begin{bmatrix} 1 & 0 & 0 \\ 0 & cos(\vartheta(t)) & -sin(\vartheta(t)) \\ 0 & sin(\vartheta(t)) & cos(\vartheta(t)) \end{bmatrix}$.

The accelerations of the relative pendulum coordinates are

$$\begin{Bmatrix} \ddot{x} \\ \ddot{y} \\ \ddot{z} \end{Bmatrix} = L_p \frac{d^2}{dt^2} \begin{Bmatrix} sin(\psi(t)) \\ cos(\psi(t))sin(\vartheta(t)) \\ cos(\vartheta(t))sin(\psi(t)) \end{Bmatrix} \tag{3}$$

In the solution of the Eq. (3) there is a substitute $\frac{d\vartheta}{dt} = p$ and $\frac{d\psi}{dt} = q$.

Dynamic equilibrium is described by conservation of momentum about two independent axes of rotation (along and perpendicular to the wire): and, leading to two second order differential equations (see Goldstein *et al.* 2001) for 'classic 'pendulum angles only). The equations are formulated as equilibrium of internal and external momentum, according to the d'Alembert principle

$$\vec{N}_i = \vec{N}_g \tag{4}$$

where $\vec{N}_i$ is the internal and $\vec{N}_g$ the external momentum due to gravity. Further

$$\vec{N}_i = \left(E_\psi F_\vartheta\right)\left(\begin{Bmatrix} x \\ y \\ z \end{Bmatrix} \times m \begin{Bmatrix} \ddot{x} \\ \ddot{y} \\ \ddot{z} \end{Bmatrix}\right), \quad \vec{N}_g = \left(E_\psi F_\vartheta\right)\left(\begin{Bmatrix} x \\ y \\ z \end{Bmatrix} \times \begin{Bmatrix} 0 \\ 0 \\ -mg \end{Bmatrix}\right) \tag{5}$$

After the appropriate substitutions, we obtain four normalised differential equations $\frac{d}{dt}\begin{Bmatrix} \vartheta \\ \psi \\ p \\ q \end{Bmatrix} = \begin{Bmatrix} p \\ q \\ DEP_1 \\ DEP_2 \end{Bmatrix}$ where DEP_i are pendulum differential equations.

2.3 The combined model

The combination of the two models is based on Goldstein, Poole and Safko (2001); it combines the influence of the mass sliding along an extensible wire with a 3D pendulum model. In addition, the pendulum origin moves and accelerates as it slides along the rope. We have to modify the existing equations and the Eq. (1) becomes

$$\begin{Bmatrix} \ddot{a} \\ \ddot{Y} \\ \ddot{F} \end{Bmatrix} = \begin{Bmatrix} DE_1 \\ DE_2 \\ DE_3 \end{Bmatrix} - \begin{Bmatrix} \ddot{x} \\ \ddot{y} \\ \ddot{z} \end{Bmatrix} \tag{6}$$

where DE_i are differential equations describing changes in position along the wire. {*x*,*y*,*z*} are

pendulum coordinates which must be related to the coordinates of the point on the wire. The momentum balance Eq. (4) now gets an additional term $\vec{N}_i = \vec{N}_g + \vec{N}_a$ that introduces the motion and acceleration of the origin of the pendulum

$$\vec{N}_a = \left(E_\psi F_\vartheta\right)\left(\begin{Bmatrix} x \\ y \\ z \end{Bmatrix} \times \begin{Bmatrix} \ddot{a} \\ \ddot{Y} \\ \ddot{F} \end{Bmatrix}\right) \tag{7}$$

After combining the above equations and introducing the necessary transformations, our model is described by a system of 5 second order (or 10 normalized-first order) nonlinear differential equations with suitable initial conditions

$$\begin{Bmatrix} \ddot{a} \\ \ddot{Y} \\ \ddot{F} \\ \dot{p} \\ \dot{q} \end{Bmatrix} = \begin{Bmatrix} DE_1 - \ddot{x} - fric(a) \\ DE_2 - \ddot{y} \\ DE_3 - \ddot{z} \\ DE_4 \\ DE_5 \end{Bmatrix} \tag{8}$$

Here $DE_4 = \frac{d(\vec{N}_i - \vec{N}_g - \vec{N}_a)}{d\vartheta}$, $DE_5 = \frac{d(\vec{N}_i - \vec{N}_g - \vec{N}_a)}{d\psi}$ and we have introduced the frictional force, "$fric(a)$". We see that it is possible to introduce the frictional force as a function of any available parameter (here the distance 'a'). However, it is not easy to determine its functional form.

For the solution procedure, Eq. (8) is expanded into the normalised system of 10 first order differential equations with 3 additional variables

$$\begin{Bmatrix} u \\ v \\ w \end{Bmatrix} = \begin{Bmatrix} \dot{a} \\ \dot{Y} \\ \dot{F} \end{Bmatrix} \tag{9}$$

Here, u, v, w are additional variables (besides 'p' and 'q'). Numerical calculations are performed using Wolfram Mathematica 2022 numerical solver 'NDSolve' with settings: Method->"EquationSimplification"->"Solve" and MaxSteps->100000.

2.4 The initial conditions

The initial conditions determine the dependent parameters, given the initial position of the load (pendulum). One gives the initial (starting) position on the rope 'a' and lateral distance 'Y' and finds compatible sag/displacement 'F'; together they then form the initial conditions. In Fig. 3(a) we see dependance of the balance residual on the sag 'F' in the initial condition balance Eq. (10). Initially, it is determined from two nonlinear equations with unknown total sag F and wire tension force T. One equation describes the total length of the rope (including elastic elongation) and the other describes the force balance at the load position. It is possible to combine the two equations into one by inserting the length constraint into the force balance. The resulting equation describing the balance between the pendulum mass and the corresponding rope/cable geometry is

$$mg = EA(L1 + L2 - 1)\left(\frac{F}{L1} + \frac{F-h}{L2}\right) \tag{10}$$

Here, $L1$ and $L2$ are functions given above. Moreover, initial condition for lateral displacement is usually zero, i.e., $Y_0 = 0$. When written in its full form Eq. (10) reveals dependence on the parameter 'a' (initial distance of the pendulum from the beginning of the rope and the parameter

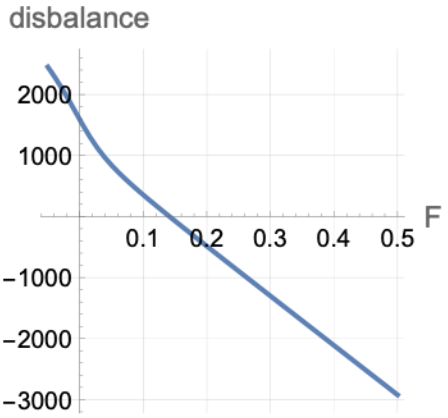

(a) sag '*F*' resulting from initial conditions for and *a*=0.1 m

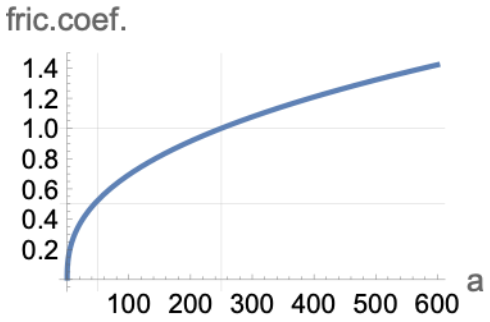

(b) friction force as function of the distance '*a*'

Fig. 3 (a) initial conditions; (b) friction force

'*F*' (the sag). One has to choose value for one of the parameters and calculate the other (in Kožar and Torić Malić 2014) is described how is the rope/cable tension force related to parameters '*a*' and '*F*'). The initial rope/cable pretension can not be inserted directly as an initial condition but is taken into account by the ratio of the chosen total cable length '*L*' and the geometric distance between the cable supports (taking into consideration cable elasticity and its cross section).

From the graphical representation of Eq. (10) one can see the nature of the nonlinearity and the approximate solution for the initial condition. In practice, Eq. (10) is solved by the secant method.

In Fig. 3 we see evolution of the frictional force used to model braking on the zip-line. It can be easily introduced into the final system of Eq. (8), but its exact form is unknown at the moment. It has been assumed to be exponential and a function of the distance 'a', with parameters adjusted to reduce the speed of sliding to approximately zero (see Fig. 5). The determination of the parameters of the braking function in advance, so that it is guaranteed to stop sliding at the end of the rope, has not yet been solved.

3. Example

This example is a dynamic recalculation of some previous designs performed with a static 2D version of the cable model used for the design of a series of zip-lines built over the river "Cetina" in Omiš, Croatia. The zip-lines varied in length, from 180 to 700 meters, and a few of them were without sag. The sag is an indicator of the magnitude of the static force present in the rope/cable, which is an important parameter for the resulting mass velocity. Although it is condensed in the final system of equations, it is important for the assessment of results because it is easily measured. At this point I would like to emphasise the role of the tension force in the rope/cable. Although it is deleted from the equations to reduce its number, it is important because its static value can be easily measured. The measured value can be used to estimate the geometry parameters of the rope/cable, since the length and height measurements in the field are prone to error. In Fig. 4 (left) we see an example of rope/cable tensile force measurement due to self weight and static load. In Fig. 4 (right) we see the tension cell connected to the data logger hanging from a

Fig. 4 Tension force measurement due to static loading (left), force and acceleration measurement on the pendulum attachment point (right)

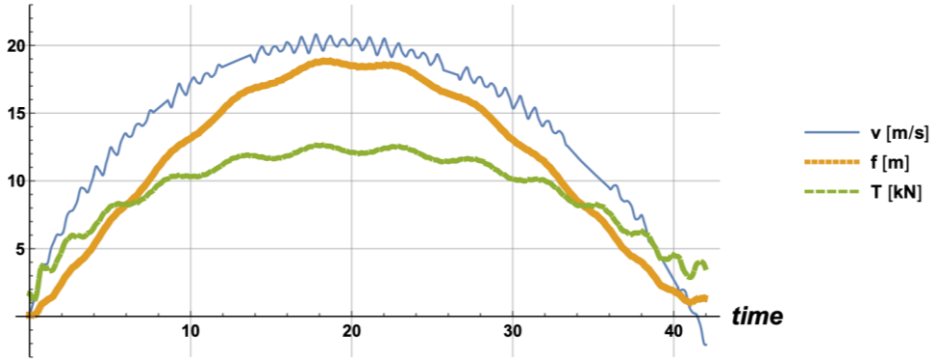

Fig. 5 Pendulum kinematics in 3D

person during zip-line flight and a 3-axial acceleration sensor.

The numerical example was calculated with Wolfram Mathematica 2022 with realistic parameters from the zip-line: EA=6 MN, m=150 kg, l=600 m, h=60 m, L=602.9 m, Lp=0.1 m. The first 42 seconds of the simulation are shown in Figs. 5, 6, and 7. Fig. 5 shows the change in sliding speed, the vertical position on the rope (at the point of pendulum suspension) and the tension force in the rope. This dynamic tension force can be compared with the measured static tension force (see Fig. 4). Although they are different, their comparison is a good guide for design. Fig. 6 shows the trajectories of the pendulum suspension point (on the rope) and the pendulum mass with displacement 'Y' exaggerated by an unknown factor (the size of the drawing frame for the image has been specified and filled in for maximum visibility). Fig. 7 (left) shows an envelope of the pendulum suspension point along the sliding path and Fig. 7 (right) shows the swinging of the mass on the pendulum during sliding.

3.1 Solutions

Fig. 7 (left) is a lateral projection of Fig. 5. Each point on this figure should be connected by a straight line to the rope/cable supports, which would obscure the figure and is therefore not included. This data could be measured with the GPS locator, but this requires a professional instrument with a sampling rate of at least 10 samples/second. From Fig. 7 (right), it can be

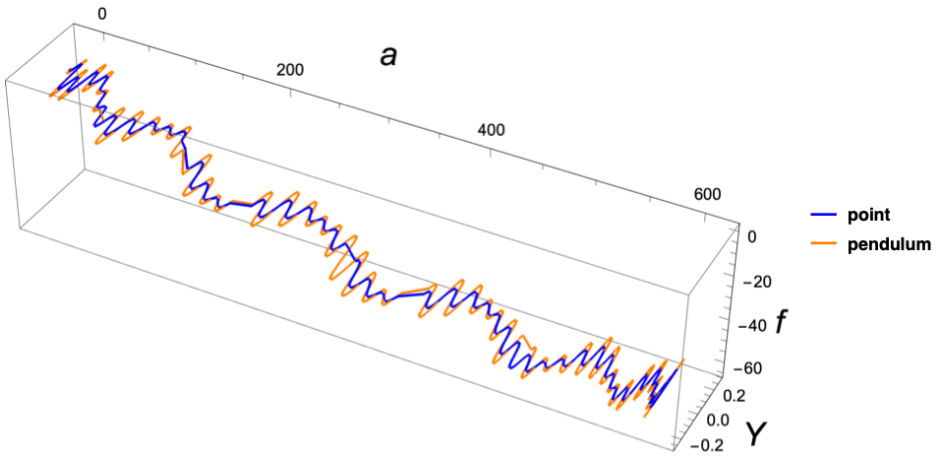

Fig. 6 Comparison of displacements of the point on the rope and the mass of the pendulum

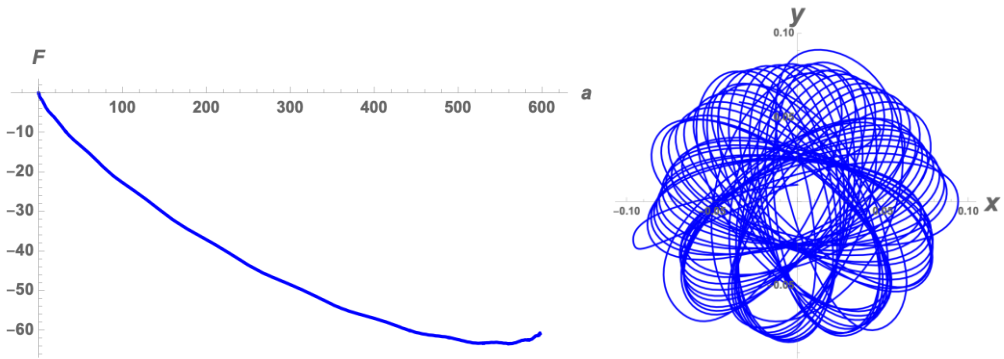

Fig. 7 (left) Side view of the rope envelopes during mass sliding, (right) top view of the pendulum mass during sliding

estimated that the pendulum motions are less than 10 cm. This is important data, because the accelerations of a person on the rope can be measured and the displacements can be extracted from it, so that these data can also be used for parameter calibration in the design of the zip-line.

4. Validation

The author has carried out a preliminary validation of the model by comparing the calculated and measured forces in the pendulum. Since the mass of the pendulum is known, we need its acceleration to determine the force, which is the difference between the weight of the mass and its acceleration force in the direction of the rod. The direction of the rod is constantly changing, but its angle is calculated, i.e., known (see Eqs. (8) and (9)).

The measurements of the force in the rod are carried out on site using the AHLBORN equipment, the battery-operated data logger 2690 and the force sensor K-25 with a maximum permissible force of 5 kN, see Fig. 8. The force is sampled 50 times per second, i.e., 2000 samples for 40 seconds of measurement time. Before comparison, the measurement data is smoothed using

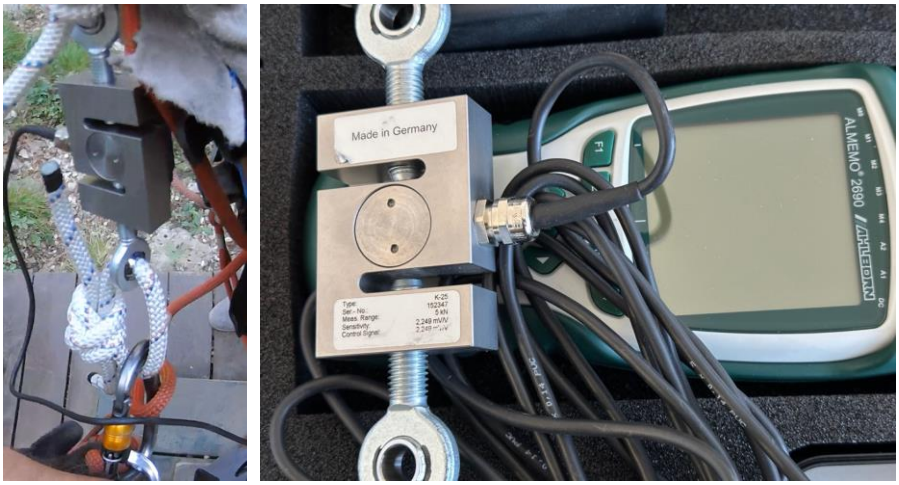

Fig. 8 Measuring equipment for the force in the pendulum rod

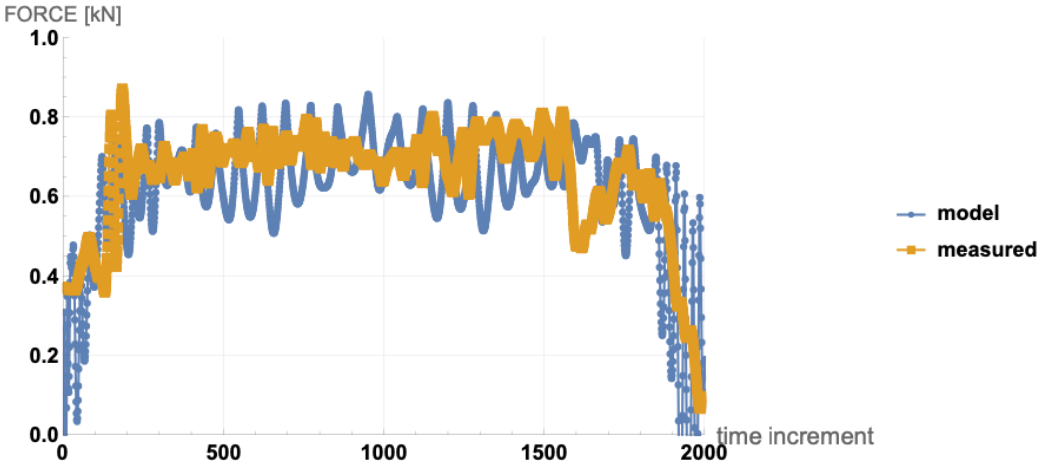

Fig. 9 Comparison of various parameters in the result

the cosine Fourier transform, but this only contributes to better visibility, no significant peaks are removed. The pendulum simulates a person hanging from the zip line, and the real-time measurement of the rod force can easily be made by a person sliding along a rope and carrying the measuring equipment.

The measurements are carried out on the zip line in Omis, Croatia. There are 8 rope slides of different lengths, from 180 to 700 meters. The example shown in Fig. 9 refers to rope slide no. 4 with a horizontal span of 262 meters and a height of 41 meters, which consists of a compacted steel rope with a diameter of 12 mm.

The system of corresponding differential equations is solved and the acceleration components are determined, from which the force of the pendulum rod is calculated. The comparison between the model prediction and the measured data is shown in Fig. 9.

All 8 zip lines matched the model very well, but the detailed analysis will be the subject of another paper (as can be seen from Fig. 4, additional parameters were measured).

5. Conclusions

The model based on a system of algebraic differential equations is quite successful in modelling the sliding of mass along a rope. The presented model alleviates the problem of modelling a moving load by including its position in the system variables. This model can be further discretized using any method as long as the moving load is taken into account. A numerical example illustrates the successful implementation of the model. Furthermore, the model was verified on the examples of a sliding mass without pendulum and a fixed pendulum expressed by 'classical' angles and by angles υ and ψ. Furthermore, the model can serve as a good basis for a parametric analysis, which could facilitate the design of a cableway and give a better insight into the behaviour of a rope under moving load. Furthermore, the model results could be related to some data that are relatively easy to measure in the field and thus could be used for parameter calibration and quick and easy estimation of the safety of the ropeway during operation.

In the future, the modelling of the brake will be analysed to mimic human behaviour when stopping at the end of the rope; currently it is based on an estimate of a friction parameter. It is also planned to modify the equations to take into account ropes/cables whose dead weight is not negligible (i.e., long ropes and ropes with low tensile force).

Acknowledgments

This work was supported by projects uniri-tehnic-18-108-1245 and uniri-tehnic-23-176-3146, for which we gratefully acknowledge.

References

Baillieul, J. (1985), "Kinematic programming alternatives for redundant manipulators", *IEEE International Conference on Robotics and Automation*, St. Louis, MO, USA. https://doi.org/10.1109/ROBOT.1985.1087234.

Burov, A.A. and Nikonov, V.I. (2024), "Dynamics of a heavy pendulum of variable length with a movable suspension point", *Acta Mechanica*, 1-9. https://doi.org/10.1007/s00707-024-03926-x.

Costa, L.G. and Savi, M.A. (2024), "Pendulum-based hybrid system for multidirectional energy harvesting", *Nonlin. Dyn.*, **112**(21), 18665-18684. https://doi.org/10.1007/s11071-024-10040-z.

Coulibaly, J.B., Chanut, M.A., Lambert, S. and Nicot, F. (2018), "Sliding cable modeling: An attempt at a unified formulation", *Int. J. Solid. Struct.*, **130**, 1-10. https://doi.org/10.1016/j.ijsolstr.2017.10.025.

Goldstein, H., Poole, C.P. and Safko, J.L. (2001), *Classical Mechanics*, Addison-Wesley.

Golub, A.P., Klimina, L.A., Lokshin, B.Y. and Selyutskiy, Y.D. (2023), "Autooscillations of a multlink aerodynamic pendulum", *J. Comput. Syst. Sci. Int.*, **62**(2), 280-289. https://doi.org/10.1134/S1064230723020089.

Ibrahimbegovic, A., Mejia-Nava, R.A., Hajdo, E. and Limnios, N. (2022), "Instability of (Heterogeneous) Euler beam: deterministic vs. stochastic reduced model approach", *Couple. Syst. Mech.*, **11**(2), 167-198. https://doi.org/10.12989/csm.2022.11.2.167.

Kožar, I. and Torić Malić, N. (2014), "Analysis of body sliding along cable", *Couple. Syst. Mech.*, **3**(3), 291-304. https://doi.org/10.12989/csm.2014.3.3.291.

Kožar, I., Lozzi Kožar, D. and Torić Malić, N. (2022), "Simple factor analysis of measured data", *Couple. Syst. Mech.*, **11,** 33-41. https://doi.org/10.12989/csm.2022.11.1.033.

Mourid, E., Mamouri, S., Kouli, R. and Ibrahimbegovic, A. (2022), "An efficient implicit time stepping

scheme for nonlinear dynamics analysis of 3D geometrically exact beam using exponential mapping", *Mech. Adv. Mater. Struct.*, **29**(28), 7189-7203. https://doi.org/10.1080/15376494.2021.1994062.

Nguyen, C.U., Hoang, T.V., Hadzalic, E., Dobrilla, S., Matthies, H.G. and Ibrahimbegovic, A. (2022), "Viscoplasticity model stochastic parameter identification: Multi-scale approach and Bayesian inference", *Couple. Syst. Mech.*, **11**(5), 411. https://doi.org/10.12989/csm.2022.11.5.411.

Ren, T., Zuo, J., Xu, L., Li, L. and Wang, X. (2024), "An assembly system for inertial pendulum components in miniature wire suspended pendulum accelerometers", *J. Mech. Sci. Technol.*, 1-12. https://doi.org/10.1007/s12206-024-0527-9.

Rukavina, T. and Kožar, I. (2017), "Analysis of two time-delayed sliding pendulums", *Eng. Rev.*, **37**, 11-19.

Suljevic, S., Ibrahimbegovic, A., Karavelic, E. and Dolarevic, S. (2022), "Meso-scale based parameter identification for 3D concrete plasticity model", *Couple. Syst. Mech.*, **11**(1), 55-78. https://doi.org/10.12989/csm.2022.11.1.055 55.

Wolfram Research Inc. (2022), Mathematica. https://www.wolfram.com/mathematica/.

Zhou, B., Accorsi, M.L. and Leonard, J.W. (2004), "Finite element formulation for modeling sliding cable elements", *Comput. Struct.*, **82**, 271- 280. https://doi.org/10.1016/j.ijsolstr.2021.111290.

AI